第 32 卷第 6 期 无 机 化 学 学 报 Vol.32 No.6
2016 年 6 月 CHINESE JOURNAL OF INORGANIC CHEMISTRY 1078-1088

基于 *N*-乙酰-*L*-酪氨酸构筑的两例纯手性钴(Ⅱ)配合物的合成、结构及性质

马 宁 宋会花* 于海涛
(河北师范大学化学与材料科学学院,石家庄 050024)

摘要:利用手性配体 *N*-乙酰-*L*-酪氨酸(Hacty)与钴盐通过溶液法合成了 2 例纯手性配合物{[Co(acty)(bpp)$_2$(H$_2$O)$_2$](NO$_3$)·2H$_2$O}$_n$ (**1**)和{[Co$_2$(acty)$_2$(bpe)$_3$(H$_2$O)$_3$](ClO$_4$)$_2$·4H$_2$O}$_n$ (**2**)(bpp=1,3-联(4-吡啶)丙烷,bpe=1,2-联(4-吡啶)乙烷),并对它们进行了元素分析(EA)、红外光谱(IR)、紫外光谱(UV)、热重(TG)、粉末 X 射线衍射(PXRD)及 X 射线单晶衍射测定。配合物 **1** 属于单斜晶系 $P2_1$ 空间群,六配位的 Co(Ⅱ)离子被 bpp 配体连接形成一维右手螺旋链结构。配合物 **2** 属于三斜晶系 $P\bar{1}$ 空间群,六配位的双核 Co(Ⅱ)离子被 bpe 配体连接形成一维带状链结构。在氢键的作用下,它们均形成三维超分子结构,深入讨论了不同构型的含 N 辅助配体对配合物结构的影响。此外,测定了 2 例手性配合物的圆二色(CD)光谱。

关键词:钴配合物;*N*-乙酰-*L*-酪氨酸;晶体结构;纯手性配合物
中图分类号:O614.81$^+$2 **文献标识码**:A **文章编号**:1001-4861(2016)06-1078-11
DOI:10.11862/CJIC.2016.127

Syntheses, Crystal Structures and Properties of Two Homochiral Co(Ⅱ) Complexes Based on N-Acetyl-*L*-tyrosine

MA Ning SONG Hui-Hua* YU Hai-Tao
(*College of Chemistry and Material Sciences, Hebei Normal University, Shijiazhuang* 050024, *China*)

Abstract: Two novel homochiral coordination polymers based on *N*-acetyl-*L*-tyrosine (Hacty), {[Co(acty)(bpp)$_2$(H$_2$O)$_2$](NO$_3$)·2H$_2$O}$_n$ (**1**) and {[Co$_2$(acty)$_2$(bpe)$_3$(H$_2$O)$_3$](ClO$_4$)$_2$·4H$_2$O}$_n$ (**2**) (bpp=1,3-di(4-pyridyl)propane, bpe=1,2-di(4-pyridyl)ethane) have been synthesized and characterized by elemental analyses, IR, UV, TG, PXRD, single-crystal X-ray diffraction. Complex **1** crystallizes in the monoclinic space group $P2_1$, and the six-coordinated Co(Ⅱ) ions are bridged by bpp ligands, exhibiting a 1D right-handed helical chain structure. Complex **2** belongs to the triclinic space group $P\bar{1}$, and the six-coordinated dinuclear Co(Ⅱ) ions are bridged by bpe ligands, forming a 1D ribbon chain structure. The two different 1D chains are further extended into 3D supramolecular architectures through hydrogen-bonding interactions. The effect of different N-donor ancillary ligands on the structural assembly and diversity has been further discussed. Furthermore, circular dichroism spectra (CD) of compounds **1** and **2** were investigated. CCDC: 1438882, **1**; 1438883, **2**.

Keywords: cobalt(Ⅱ) complex; *N*-acetyl-*L*-tyrosine; crystal structure; homochiral complex

收稿日期:2015-12-17。收修改稿日期:2016-04-15。
国家自然科学基金(No.21141002)和河北省自然科学基金(No.B2012205040)资助项目。
*通信联系人。E-mail:songhuihua@mail.hebtu.edu.cn

0 Introduction

The rational design and controlled synthesis of chiral coordination polymers has attracted great interest owing to their intriguing structures[1-3] and their potential applications in asymmetrical catalysis, chiral separation, luminescence, magnetism and nonlinear optical applications[4-8]. Although a major challenge in this approach is the chance of the polymeric structures since many factors such as the solvent system, ligand-to-metal ratios, temperature, coordination geometry of the metals, nature of the ligands, pH value of solution[9-14], the internal surface functionality and topology of chiral complexes could be crafted efficiently by choosing appropriate ligands and metal ions with diverse coordination geometry under optimum reaction conditions. Recently, numbers of chiral coordination polymers with aesthetic structural motifs and potential applications have been obtained by using multidentate ligands[15-16].

According to previously reported, the usage of chiral ligands as reactant precursors is one of the most efficient and viable approaches for the homochiral coordination polymers[17-18]. Chiral amino acid derivatives as good candidates for construction of chiral coordination polymers, have attracted considerable attention due to their coordination sites and rich bonding modes[19-21]. *N*-acetyl-*L*-tyrosine can donate carboxylic group, which could adopt versatile coordination modes, including monodentate, bidentate chelating and bridging to give high dimensional structure. From the viewpoint of crystal supramolecular structure, *N*-acetyl-*L*-tyrosine creates countless possibilities for the formation of inter- and intramolecular interactions through aromatic interactions and hydrogen bonds to stabilize the structure of chiral coordination polymers. However, only a few examples of chiral coordination polymers with Hacty have been reported[22-23].

Apart from the amino acid derivative linker, N-donor ancillary ligands also play an important role in structural assembly and diversity of the coordination polymers. Herein, the second N-donor ligands with different conformations and lengths such as 1,3-di(4-pyridyl)propane and 1,2-di(4-pyridyl)ethane were employed respectively and we have gained two homochiral complexes, namely, $\{[Co(acty)(bpp)_2(H_2O)_2](NO_3)\cdot 2H_2O\}_n$ (**1**) and $\{[Co_2(acty)_2(bpe)_3(H_2O)_3](ClO_4)_2\cdot 4H_2O\}_n$ (**2**) (bpp=1,3-di(4-pyridyl)propane, bpe=1,2-di(4-pyridyl)ethane). Bpp and bpe ligands all can be found as two geometric isomers in titled complexes, respectively (Scheme 1). More importantly, the simultaneous appearance of two different conformations of bpp or bpe ligands in one crystal structure is rarely reported. Herein we report their syntheses, crystal structures and circular dichroism spectra (CD). Furthermore, the effects of N-donor ligands on the structures of the complexes have been discussed in detail.

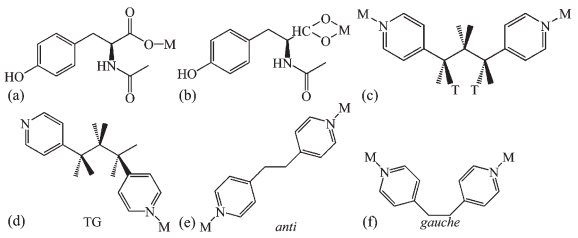

Scheme 1　(a) Observed coordination mode of Hacty ligand for **1** and **2**; (b) Observed coordination mode of Hacty ligand for **2**; (c), (d) Observed coordination modes of bpp ligand for **1**; (e), (f) Observed coordination modes of bpe ligand for compound **2**

1 Experimental

1.1 Materials and methods

All reagents and solvents for syntheses were purchased from commercial sources and were used as received without further purification. Element analyses (C, H and N) were performed on an Elemental Vario EL elemental analyzer. Infrared (IR) spectra were measured on a FTIR-8900 spectrometer from 4 000 to 400 cm^{-1} (KBr pellets). Thermogravimetric analyses (TGA) were carried out on a simultaneous STA 449F3/TENSOR 27 thermal analyzer under nitrogen with a heating rate of 10 ℃·min^{-1} from room temperature to 800 ℃. Powder X-ray diffraction (PXRD) patterns were collected on a Bruker D8-Advance X-ray diffractometer using Cu $K\alpha$ radiation

(λ=0.154 2 nm, U=40 kV, I=40 mA) and ω-2θ scan mode at 293 K. The solid state circular dichroism (CD) spectra were recorded on a JASCOJ-810 spectropolarimeter with KCl pellets. Fluorescence spectra were recorded on a Hitachi F-4500 luminescence spectrometer.

1.2 Synthesis

1.2.1 $\{[Co(acty)(bpp)_2(H_2O)_2](NO_3)\cdot 2H_2O\}_n$ (**1**)

Hacty (0.1 mmol, 0.022 3 g) was stirred into a 10 mL aqueous solution. The solution was adjusted to pH=5.6 with the addition of 1 mol·L^{-1} NaOH solution. $Co(NO_3)_2\cdot 6H_2O$ (0.1 mmol, 0.029 1 g) was added to the solution, which was heated in a water bath at 60 ℃ for about 10 min. A solution of bpp (0.2 mmol, 0.039 6 g) in MeOH (5 mL) was slowly added. The resulting solution was stirred for 10 minutes, filtered off and allowed to stand for one week. The light red block-shaped transparent crystals **1**, suitable for X-ray analysis were obtained with 51% yield based on Co. Anal. Calcd. for $C_{37}H_{48}CoN_6O_{11}$(%): C, 54.75; H, 5.96; N, 10.35. Found(%): C, 54.88; H, 5.91; N, 10.36. IR (KBr, cm^{-1}): 3 246(b), 1 614(s), 1 558(s), 1 516(s), 1 426(s), 1 384(s), 1 331(s), 1 264(s), 1 227(m), 1 179(w), 1 123(w), 1 070(m), 1 020(m), 964(w), 840(m), 818(s), 742(w), 616(w), 521(m).

1.2.2 $\{[Co_2(acty)_2(bpe)_3(H_2O)_3](ClO_4)_2\cdot 4H_2O\}_n$ (**2**)

Compound **2** was synthesized in a procedure similar to that for **1** except that $Co(ClO_4)_2\cdot 6H_2O$ (0.1 mmol, 0.036 6 g) and bpe (0.1 mmol, 0.018 4 g) was used instead of $Co(NO_3)_2\cdot 6H_2O$ and bpp, respectively. The red block-shaped transparent crystals **2** were obtained with 50% yield based on Co. Anal. Calcd. for $C_{58}H_{74}Cl_2Co_2N_8O_{23}$ (%): C, 48.38; H, 5.18; N, 7.78. Found(%): C, 49.59; H, 5.30; N, 7.91. IR (KBr, cm^{-1}): 3 361(b), 1 656(s), 1 617(s), 1 580(s), 1 427(s), 1 377(m), 1 295(w), 1 252(m), 1 100(s), 1 019(m), 878(w), 824(s), 699(w), 625(m), 528(m).

1.3 X-ray crystallography

Suitable single crystals for title compounds were selected for single-crystal X-ray diffraction analyses (Crystal size / mm: 0.31×0.24×0.11 for **1**; 0.42×0.27×0.24 for **2**). Crystallographic data were collected at 100 K for **1** and 298(2) K for **2** on a Bruker Smart Apex CCD diffractometer with graphite monochromated Mo $K\alpha$ radiation (λ=0.071 073 nm). All structures were solved through direct methods and refined by full-matrix least-squares on F^2 with SHELXL-97 program[24]. All non-hydrogen atoms were refined anisotropically. The hydrogen atoms were added theoretically and refined with a riding model. The assignment of the absolute structures for **1**~**2** was confirmed by the refinement of the Flack parameter to values of −0.005 (11) and −0.03 (2), respectively[25-26]. Oxygen atoms from ClO_4^-, carbon atoms and hydrogen atoms from bpe ligands were disordered in complex **2**. Further crystallographic data and experimental details for structural analyses of complexes **1**~**2** are summarized in Table 1. The selected bond lengths and angles of **1**~**2** are given in Table 2.

CCDC: 1438882, **1**; 1438883, **2**.

Table 1 Crystal data and structure refinements for complexes 1 and 2

Complex	1	2
Empirical formula	$C_{37}H_{48}CoN_6O_{11}$	$C_{58}H_{74}Cl_2Co_2N_8O_{23}$
Formula weight	811.74	1 440.01
Crystal system	Monoclinic	Triclinic
Space group	$P2_1$	$P\bar{1}$
a / nm	1.254 83(5)	1.144 71(1)
b / nm	1.023 97(4)	1.232 08(1)
c / nm	1.537 33(6)	1.343 31(1)
α / (°)	90	69.510 0(1)
β / (°)	90.421(3)	75.769 0(1)
γ / (°)	90	86.828(2)
Volume / nm^3	2.540 1(1)	1.719 3(3)

Continued Table 1

Z	2	1
D_c / (g·cm^{-3})	1.365	1.391
Absorption coefficient / mm^{-1}	0.5	0.639
F(000)	854	750
θ range / (°)	3.10~26.37	2.44~25.02
Reflections collected, unique	9 633, 5 334 (R_{int}=0.028 8)	8 644, 7 258 (R_{int}=0.022 2)
Refinement method	Full-matrix least-squares on F^2	Full-matrix least-squares on F^2
Data, restraints, parameters	5 334, 1, 498	7 258, 3, 933
Goodness-of-fit on F^2	1.029	1.018
R_1, wR_2 [$I>2\sigma(I)$]	0.031 9, 0.070 7	0.063 6, 0.165 2
R_1, wR_2 (all data)	0.035 7, 0.073 6	0.096 3, 0.191 6
Largest diff. peak and hole / (e·nm^{-3})	454 and −342	661 and −930

Table 2　Selected bond lengths (nm) and angles (°) for complexes 1 and 2

		1			
Co(1)-O(11)	0.208 0(2)	Co(1)-N(2)	0.214 4(2)	Co(1)-N(6)$^{\#1}$	0.215 5(2)
Co(1)-O(1)	0.208 5(2)	Co(1)-O(10)	0.215 10(2)	Co(1)-N(3)	0.216 9(2)
O(11)-Co(1)-N(3)	90.17(9)	O(1)-Co(1)-N(3)	91.77(9)	O(11)-Co(1)-O(10)	87.48(7)
O(11)-Co(1)-O(1)	177.06(8)	N(2)-Co(1)-N(3)	94.90(9)	O(1)-Co(1)-O(10)	90.33(7)
O(11)-Co(1)-N(2)	93.35(8)	O(10)-Co(1)-N(3)	89.70(8)	N(2)-Co(1)-O(10)	175.33(8)
O(1)-Co(1)-N(2)	88.68(8)	N(6)$^{\#1}$-Co(1)-N(3)	175.15(1)	O(11)-Co(1)-N(6)$^{\#1}$	93.70(9)
N(2)-Co(1)-N(6)$^{\#1}$	87.79(9)	O(10)-Co(1)-N(6)$^{\#1}$	87.56(8)	O(1)-Co(1)-N(6)$^{\#1}$	84.25(9)
		2			
Co(1)-O(9)	0.208 3(7)	Co(1)-N(5)	0.211 8(8)	Co(2)-N(8)	0.213 9(9)
Co(1)-O(17)	0.211 5(7)	Co(1)-N(3)	0.219 3(9)	Co(2)-O(14)	0.219 1(6)
Co(1)-O(18)	0.211 5(6)	Co(1)-N(7)$^{\#1}$	0.219 8(8)	Co(2)-O(13)	0.220 2(7)
Co(2)-O(19)	0.204 0(8)	Co(2)-N(4)	0.211 9(8)	Co(2)-N(6)	0.220 7(8)
O(9)-Co(1)-O(17)	177.5(3)	O(9)-Co(1)-N(7)$^{\#1}$	91.4(3)	N(8)-Co(2)-O(14)	91.7(3)
O(9)-Co(1)-O(18)	91.4(2)	O(17)-Co(1)-N(7)$^{\#1}$	91.1(3)	O(19)-Co(2)-O(13)	159.8(3)
O(17)-Co(1)-O(18)	88.5(3)	O(18)-Co(1)-N(7)$^{\#1}$	82.6(3)	N(4)-Co(2)-O(13)	98.9(3)
O(9)-Co(1)-N(5)	89.5(3)	N(5)-Co(1)-N(7)$^{\#1}$	93.4(3)	N(8)-Co(2)-O(13)	92.5(3)
O(17)-Co(1)-N(5)	90.7(3)	N(3)-Co(1)-N(7)$^{\#1}$	173.8(3)	O(14)-Co(2)-O(13)	59.9(2)
O(18)-Co(1)-N(5)	175.9(3)	O(19)-Co(2)-N(4)	101.1(3)	O(19)-Co(2)-N(6)	90.6(3)
O(9)-Co(1)-N(3)	88.2(3)	O(19)-Co(2)-N(8)	88.6(4)	N(4)-Co(2)-N(6)	89.1(3)
O(17)-Co(1)-N(3)	89.2(3)	N(4)-Co(2)-N(8)	94.0(3)	N(8)-Co(2)-N(6)	176.9(4)
O(18)-Co(1)-N(3)	91.2(3)	O(19)-Co(2)-O(14)	99.9(3)	O(14)-Co(2)-N(6)	85.5(3)
N(5)-Co(1)-N(3)	92.8(3)	N(4)-Co(2)-O(14)	158.4(3)	O(13)-Co(2)-N(6)	87.1(3)

Symmetry codes: $^{\#1}$ $-x+1$, $y-1/2$, $-z$ for **1**; $^{\#1}$ $x+1$, $y-1$, $z-1$ for **2**.

2　Results and discussion

2.1　Crystal structures

2.1.1　$\{[Co(acty)(bpp)_2(H_2O)_2](NO_3)\cdot 2H_2O\}_n$ (**1**)

The crystallographic analysis reveals that complex **1** crystallizes in the monoclinic space group $P2_1$ and features a 1D right-handed helical chain structure. There are one Co(Ⅱ) cation, one acty$^-$ anion, two bpp ligands, two coordinated water molecules, one NO_3^- and two lattice water molecules in the asymmetric

unit. As shown in Fig.1a, each Co(Ⅱ) cation is six-coordinated by one oxygen atom (O1) from one acty⁻ anion, two oxygen atoms (O10, O11) from two different coordinated water molecules and three nitrogen atoms (N2, N3, N6$^{\#1}$) from different bpp ligands. The N2, O1, O10, O11 atoms constitute the equatorial plane. N3, N6$^{\#1}$ occupy the apical positions. The Co-O bond lengths range from 0.208 0(2)~0.215 10(2) nm, and the Co-N bond lengths are in the range of 0.214 4(2)~0.216 9(2) nm.

As shown in Fig.1b, the acty⁻ anion acts as a decorating ligand in monodentate mode to connect one Co(Ⅱ) metal ion. The bpp ligands in **1** are of two types. One type of bpp serves as an unsymmetrical bridging ligand with TT[27] (T=*trans*) conformation (Scheme 1c) and links two different Co(Ⅱ) cations, forming a 1D right-handed helical chain structure along the *b* axis. In the TT conformation of flexible bpp ligand, the dihedral angle between the two independent pyridine moieties of each bpp ligand is 66.42°. The other type of bpp acts as a monodentate ligand with TG[27] (G=*gauche*) conformation (Scheme 1d) to connect one Co(Ⅱ) metal ion and arranges on both sides of the helical chain. The required uncoordinated NO_3^- anions are readily accommodated between the helical chain. In addition, extensive hydrogen bonds (Table 3) are observed and these helical chains are further linked together through hydrogen bonds to construct a 3D supramolecular structure (O(11)–H(11D)···O(9) 0.177 nm; O(9)–H(9B)···O(7)$^{\#5}$ 0.192 nm; O(11)–H(11E)···O(2)$^{\#7}$ 0.189 nm; O(9)–H(9A)···O(3)$^{\#4}$ 0.190 nm), as shown in Fig.1c.

2.1.2 $\{[Co_2(acty)_2(bpe)_3(H_2O)_3](ClO_4)_2\cdot 4H_2O\}_n$ (**2**)

Complex **2** presents a 1D chain structure which

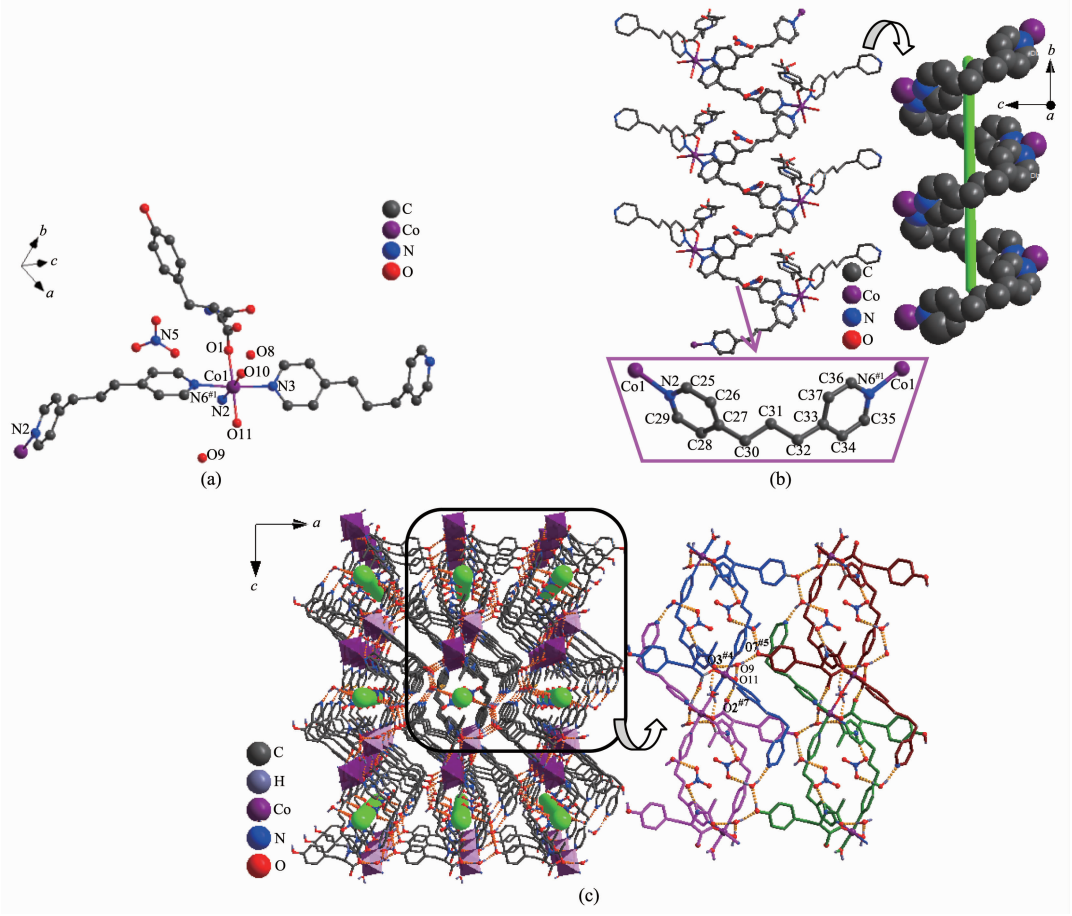

H atoms have been omitted for clarity in (a); Symmetry code: $^{\#1}$ $-x+1, y-1/2, -z$; $^{\#4}$ $x, y-1, z$; $^{\#5}$ $x+1, y-1, z$; $^{\#7}$ $-x+1, y-1/2, -z+1$

Fig.1 (a) Coordination environment of the Co center for **1**; (b) Right-handed helical chain structure in complex **1**; (c) 3D supramolecular architecture through hydrogen-bonding interactions for **1**

Table 3　Hydrogen bond lengths (nm) and bond angles (°) for complex 1

D–H···A	*d*(D-H) / nm	*d*(H···A) / nm	*d*(D···A) / nm	∠DHA / (°)
O(8)–H(8B)···O(4)$^{\#2}$	0.085	0.186	0.271 1	178
O(8)–H(8A)···N(4)$^{\#3}$	0.085	0.193	0.275 5	165
O(9)–H(9A)···O(3)$^{\#4}$	0.085	0.19	0.274 3	172
O(9)–H(9B)···O(7)$^{\#5}$	0.085	0.192	0.276 4	171
O(7)–H(7)···O(8)$^{\#6}$	0.082	0.173	0.254 6	173
O(11)–H(11E)···O(2)$^{\#7}$	0.085	0.189	0.266 2	151
O(10)–H(10A)···O(3)$^{\#7}$	0.085	0.197	0.277 5	157
N(1)–H(1A)···O(5)	0.088	0.215	0.300 7	166
O(11)–H(11D)···O(9)	0.085	0.177	0.262 2	176
O(10)–H(10B)···O(2)	0.085	0.185	0.261 7	149

Symmetry codes: $^{\#2}$ $-x+1, y+1/2, -z$; $^{\#3}$ $x, y, z-1$; $^{\#4}$ $x, y-1, z$; $^{\#5}$ $x+1, y-1, z$; $^{\#6}$ $x-1, y, z$; $^{\#7}$ $-x+1, y-1/2, -z+1$.

crystallizes in the Triclinic space group *P*1. Each crystallographic unit consists of two Co(Ⅱ) cations, two acty$^-$ anions, three bpe molecules, three coordinated water molecules, two ClO_4^- and four lattice water molecules. As shown in Fig.2a, the Co1 ion of **2** is six-coordinated and displays a slightly distorted octahedral geometry, in which the coordination sphere of Co1 is O3N3 by three nitrogen atoms (N3, N5, N7$^{\#1}$) derived from three different bpe groups, one oxygen atom (O9) from one acty$^-$ anion and two oxygen atoms(O17, O18) from two different coordinated water molecules. The Co2 ion is surrounded by three nitrogen atoms (N4, N6, N8) derived from three different bpe groups, two carboxyl oxygen atoms (O13, O14) from one acty$^-$ anion and one coordinated water molecule. The Co-O bond lengths are in the range of 0.204 0(8) ~0.220 2(7) nm. The Co-N bond lengths are in the range of 0.211 8(8)~0.220 7(8) nm.

The bpe ligands in **2** show bridging mode with *anti* and *gauche*[28] conformations (Scheme 1) alternately

Table 4　Hydrogen bond lengths (nm) and bond angles (°) for complex 2

D–H···A	*d*(D-H) / nm	*d*(H···A) / nm	*d*(D···A) / nm	∠DHA / (°)
N(1)–H(1)···O(1)	0.086	0.263	0.346 8	164
N(2)–H(2)···O(11)$^{\#9}$	0.086	0.218	0.297 8	154
O(11)–H(11)···O(21)$^{\#10}$	0.082	0.189	0.268 0	161
O(15)–H(15)···O(10)$^{\#7}$	0.082	0.180	0.262 3	177
O(17)–H(17C)···O(5)$^{\#8}$	0.085	0.198	0.282 9	174
O(17)–H(17D)···O(16)$^{\#4}$	0.085	0.183	0.267 2	173
O(18)–H(18C)···O(10)	0.085	0.191	0.275 2	174
O(18)–H(18C)···O(9)	0.085	0.252	0.300 5	117
O(18)–H(18D)···O(14)$^{\#4}$	0.085	0.187	0.271 6	175
O(19)–H(19C)···O(20)	0.085	0.178	0.262 7	172
O(19)–H(19D)···O(22)$^{\#3}$	0.085	0.184	0.268 5	173
O(20)–H(20C)···O(3)	0.085	0.230	0.315 2	176
O(20)–H(20D)···O(15)$^{\#6}$	0.085	0.196	0.281 1	176
O(21)–H(21C)···O(6)$^{\#8}$	0.085	0.223	0.304 1	160
O(21)–H(21D)···O(12)$^{\#5}$	0.085	0.193	0.273 8	160
O(22)–H(22F)···O(7)	0.085	0.230	0.286 4	124
O(23)–H(23C)···O(2)	0.085	0.214	0.286 2	142
O(23)–H(23D)···O(7)	0.085	0.190	0.261 7	141

Symmetry codes: $^{\#3}$ $x, y, z+1$; $^{\#4}$ $x, y, z-1$; $^{\#5}$ $x, y+1, z$; $^{\#6}$ $x, y-1, z$; $^{\#7}$ $x, y+1, z+1$; $^{\#8}$ $x+1, y, z$; $^{\#9}$ $x+1, y+1, z$; $^{\#10}$ $x-1, y-1, z$.

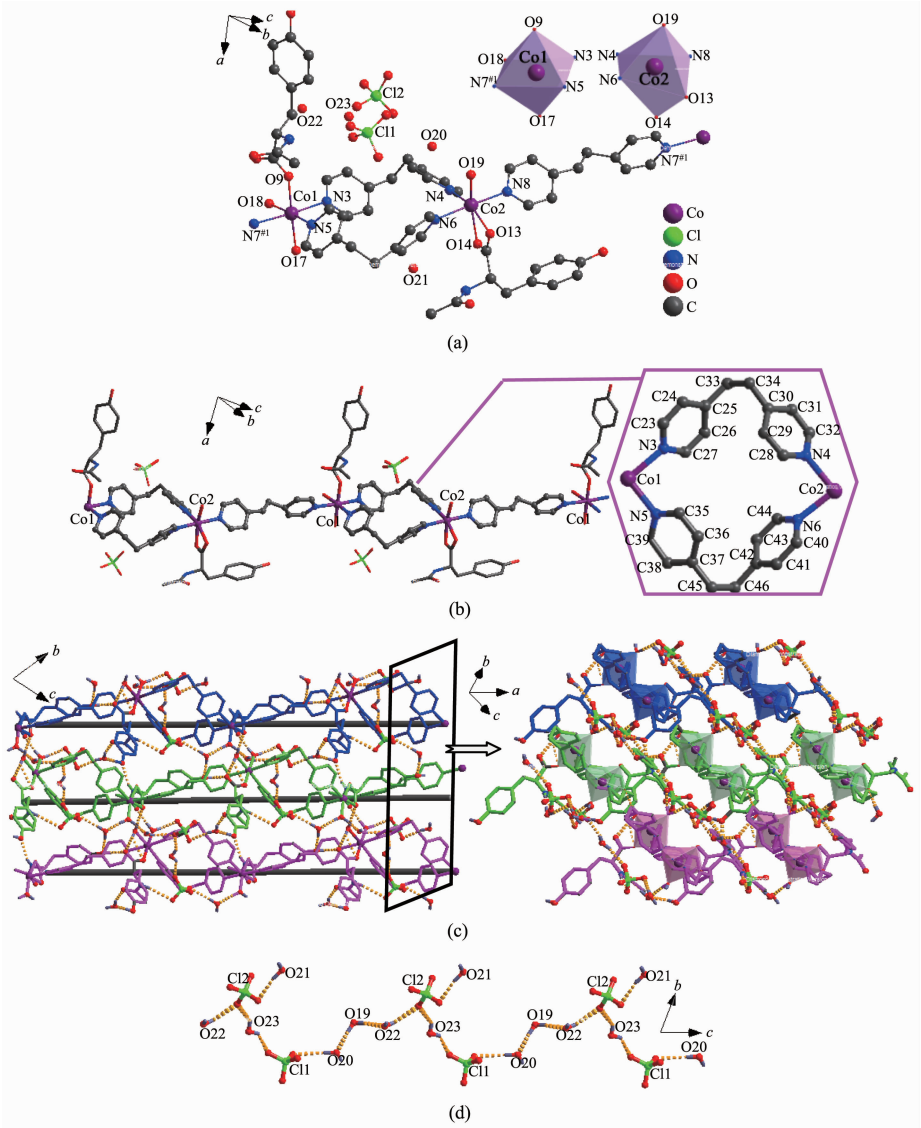

H atoms have been omitted for clarity; Symmetry code: #1 $x+1, y-1, z-1$

Fig.2 (a) Coordination environment of the Co center for **2**; (b) 1D chain structure for complex **2**; (c) 3D supramolecular architecture through hydrogen-bonding interactions for **2**; (d) Supramolecular chain through hydrogen-bonding interactions for **2**

to link adjacent Co ions to form a 1D ribbon chain structure (the bpe ligand with *anti* conformation provides a N-to-N separation with the distance of 1.372 47(2) nm and the *gauche* conformation separation is 0.965 70(2) nm). Due to the flexibility of bpe ligand, the torsion angle py-C-C-py of bpe ligand for the *gauche* conformation is in the range of 79.7(3)°~81.83° and the dihedral angle between the two independent pyridine moieties of each bpe ligand is in the range of 46.61° ~47.46° . Similar low values of the torsion angles have been found for other Co-(*gauche*-bpe)$_2$-Co chains[28]. Meanwhile, one half of acty$^-$ ligands adopt monodentate mode to connect Co1 ions arranged on one side of the chain, and the other half of acty$^-$ ligands act as chelating bidentate ligands to connect Co2 ions on the other side of the chain, as shown in Fig.2b. The adjacent 1D ribbon chains are linked to each other via O–H···O (Table 4) interactions to form a 3D supramolecular structure viewed along a axis direction, as shown in Fig.2c. Significantly, the uncoordinated ClO_4^- anions are involved in hydrogen bonding interaction with the four lattice water

molecules leading to the construction of a 1D hydrogen-bonded supramolecular chain, as shown in Fig.2d.

2.1.3　Effect of different N-donor ligands

The different structures of the two complexes with the same metal center of Co(Ⅱ) and acty$^-$ anion indicate that the different N-donor ancillary ligands have great influence on the connectivities of the complexes due to their different structures and flexibility. In this work, we select two kinds of N-donor ligands (bpp and bpe) to observe their effects on the assembly of the coordination compounds. The bpp and bpe ligands are both N-containing linkages which can provide twisty configurations. For example, the twist bpp ligand can assume two different configurations (TT and TG) owing to the orientations of -CH_2-CH_2-CH_2- groups. While the bpe ligand also can assume two different conformations (*anti* and *gauche*) that display different N-to-N distances owing to the orientations of -CH_2-CH_2- groups. The different degree of distortion is due to the different numbers of C atoms. For example, the dihedral angle between the two independent pyridine moieties is 66.42° for TG configuration of bpp ligand and in the range of 46.61°~47.46° for *gauche* configuration of bpe ligand. Further comparative analysis of the structures of the two complexes reveals that complex **1** shows a 1D right-handed helical chain structure and complex **2** shows a 1D ribbon chain structure. So from the results above, we can see that the different configurations and tortuosities of N-donor ligands play an important role in the formation of the crystal structures. Meanwhile, the coordination modes of the Hacty are different in the two complexes and only act as decorating ligands. The acty$^-$ ligand in monodentate mode connects one Co ion in complex **1**. The acty$^-$ ligands act as monodentate and chelating bidentate ligands connect Co ions in **2**. Additionally, complexes **1** and **2** self-assemble to form 3D supramolecular structures through hydrogen-bonding interactions.

2.2　UV-Vis spectra and IR spectra

The UV-Vis spectra of bpp, bpe, complexes **1** and **2** in H_2O/DMF (1∶10, *V*/*V*) solution with the concentration of 2×10^{-5} mol·L^{-1} at room temperature are shown in Fig.3. Bpp and bpe show intense absorption band at 253 and 255 nm, respectively. The absorption bands of these ligands can be assigned to the π-π transition. Complexes **1** and **2** all show intense absorption bands at 255 nm and weak bands at 274 nm. The locations of intense absorption bands of complexes **1** and **2** are almost similar to the assistant ligands, while strength of intense absorption bands are stronger than the assistant ligands, which may be due to the ligands coordinate to metal ions. The different π-π transition energies may be due to the formation of Co-N and Co-O bands, which result in the weak absorption bands[29-30].

The IR spectra (Fig.4) of the complexes show broad at about 3 246 cm^{-1} for **1**, 3 361 cm^{-1} for **2**, which can be ascribed to the presence of ν_{as}(O-H) stretching frequencies of Hacty. The ν_{as}(COO-) and ν_s(COO-) vibrations can be observed at 1 558 and

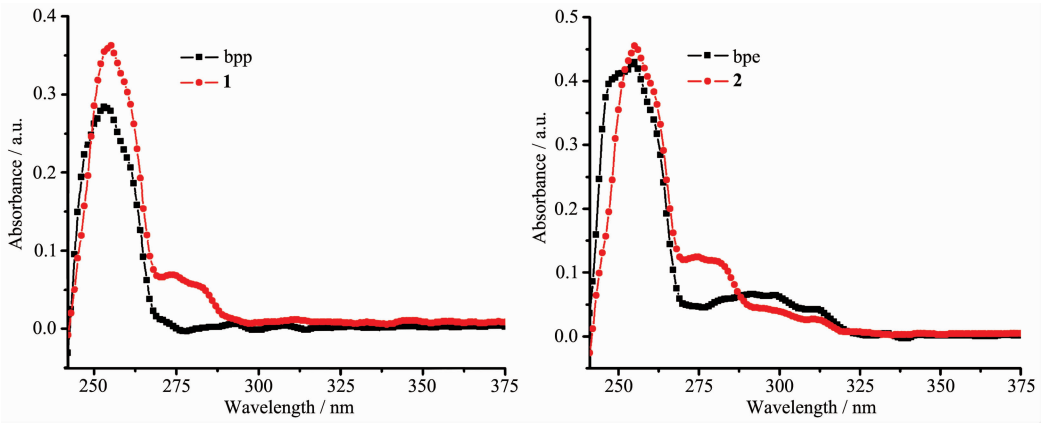

Fig.3　UV-Vis absorption spectra of complexes **1** and **2**

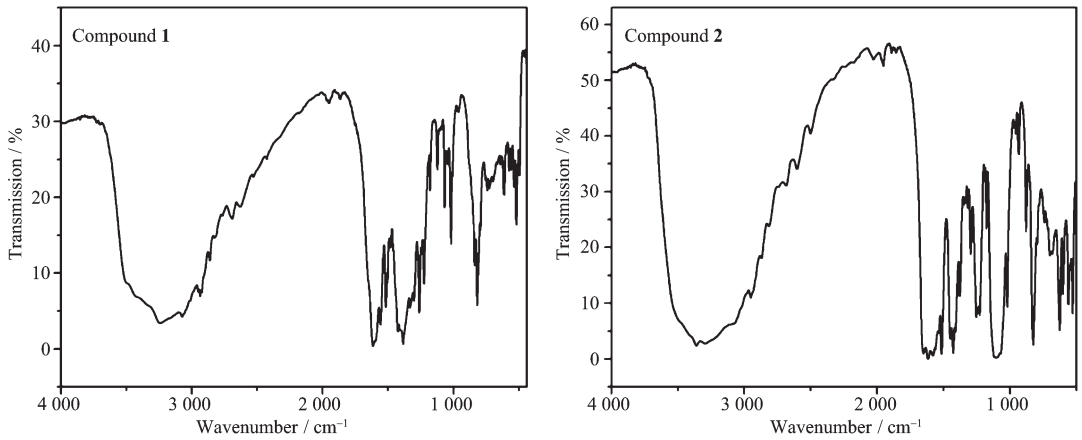

Fig.4 IR spectra of complexes **1** and **2**

1 426 cm^{-1} for **1**, 1 580 and 1 427 cm^{-1} for **2**, respectively. The IR bands of bpp at 1 384 and 1 614 cm^{-1} are due to $\nu_{C=C}$ and $\nu_{C=N}$ vibrations for compound **1**. In compound **2**, $\nu_{C=C}$ and $\nu_{C=N}$ vibrations of bpe show stretches at 1 377 and 1 617 cm^{-1} [27-28].

2.3 Thermal analysis and PXRD patterns

The thermal analysis experiments are performed on solid samples consisting of numerous single crystals in the 20~800 ℃ range under N_2 atmosphere (Fig.5). The TGA curve of **1** suggests that the first weight loss in the range of 56 ~143 ℃ corresponds to the release of two lattice water molecules and two coordinated water molecules(Obsd. 8.27 %, Calcd. 8.87 %). Above 262 ℃, compound **1** releases the organic moieties to decompose. The TGA curve of **2** suggests that the first weight loss in the range of 27 ~136 ℃ corresponds to the release of seven lattice water molecules (Obsd. 7.62 %, Calcd. 8.75 %). Compound **2** continues to lose weight up 278~800 ℃, indicating the continuous expulsion of organic moieties even at the upper limit of the measurement range. The decomposition of organic ligands of compounds **1** and **2** occur above 262 and 278 ℃, respectively, indicating that the two complexes are relatively stable.

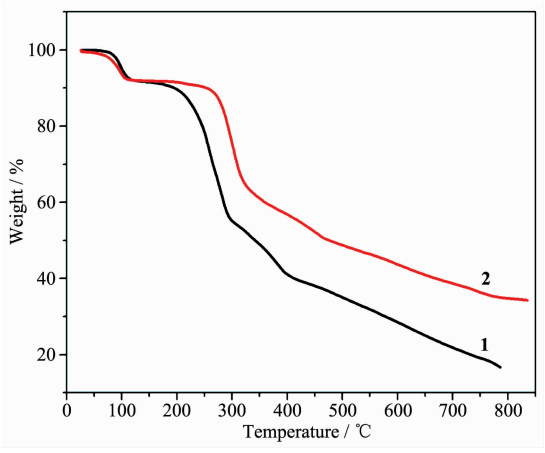

Fig.5 TGA curves of complexes **1** and **2**

To check the phase purity of the products, the powder X-ray diffraction (PXRD) experiments were carried out for **1**~**2** at room temperature. The main peaks of simulated patterns of **1**~**2** are basically consistent with their experimental patterns, demonstrating that the bulk synthesized materials and the measured single crystals are the same. The differences in intensity may be due to the preferred orientation of the crystal samples (Fig.6).

2.4 Solid-state circular dichroism (CD) spectra

To further examine the chiroptical activities, the solid-state CD (circular dichroism) spectra of the ligand Hacty and complexes **1**~**2** were measured in KCl pellet, as shown in Fig.7.

Chiral Hacty exhibits two positive bands centered at 228 and 287 nm. The CD spectrum of **1** shows two positive Cotton effect around 230 and 284 nm and a negative signal centered around 241 nm, and the spectrum of **2** shows two positive Cotton effect around 233 and 269 nm. Compounds **1** and **2** show obvious Cotton effect in the CD spectra, which confirm the chirality of the bulk materials [31]. The formation of the chiral structures of **1** and **2** have influence on the direction (+ or −) of the CD signals except for a slight

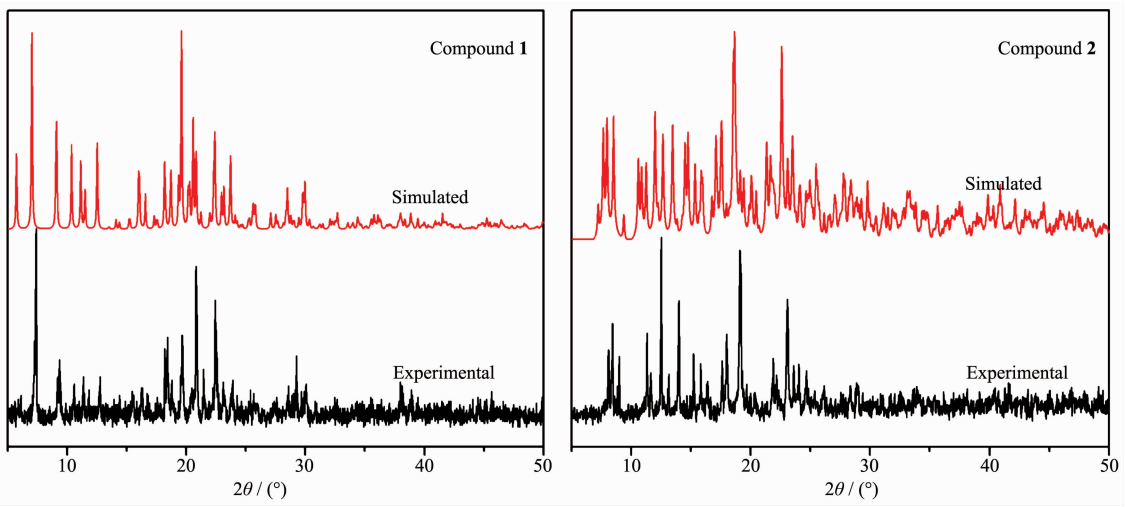

Fig.6　XRD patterns of complexes **1** and **2**

shift of the absorption peaks position compared with Hacty, which indicates the CD chromophores maybe affected by the ligand Hacty. The outcomes are in accord with the structures obtained by single crystal X-ray diffraction.

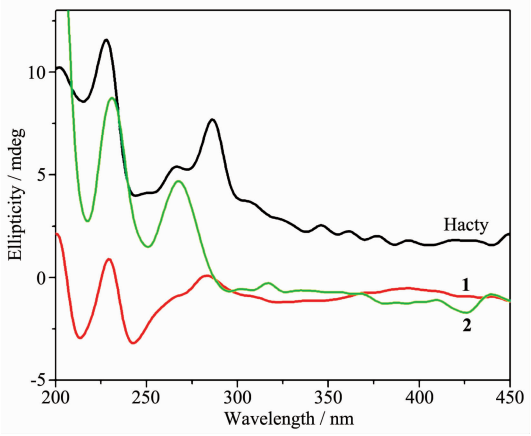

Fig.7　Solid-state CD spectra of bulk samples of the ligand Hacty and complexes **1** and **2**

3　Conclusions

In summary, we have successfully synthesized two homochiral compounds using *N*-acetyl-*L*-tyrosine under same condition. Compounds **1** and **2** show 1D right-handed helical chain and 1D ribbon chain structure, respectively. The results show that different numbers of C atoms have critical effect on the flexibilities and tortuosities of N-donor ligands (bpp and bpe), thereby different lengths and configurations of N-donor ligands directly influence the final crystal structures. 3D supramolecular structures of **1** and **2** are formed finally through hydrogen-bonding interactions to stabilize their homochiral networks. Meanwhile, *N*-acetyl-*L*-tyrosine exhibits different coordination modes. Compounds **1** and **2** are chiral complexes, and the CD spectra demonstrated that they are all homochiral. This study also reveals the significant effects of auxiliary ligands on the self-assembly of chiral compounds. Future research will further focus on the chiral synthesis, which might lead to breakthroughs in synthesis of more chiral materials.

References:

[1] Jassal A K, Sharma S, Hundal G, et al. *Cryst. Growth Des.*, **2015**,**15**:79-93

[2] Goswami A, Bala S, Pachfule P, et al. *Cryst. Growth Des.*, **2013**,**13**:5487-5498

[3] Cheng L, Zhang L M, Gou S H, et al. *CrystEngComm*, **2012**, **14**:4437-4443

[4] Zhang J, Chen S M ,Wu T, et al. *J. Am. Chem. Soc.*, **2008**, **130**:12882-12883

[5] Yokota M, Doki N, Shimizu K. *Cryst. Growth Des.*, **2006**,**6**: 1588-1590

[6] Li M, Yang J, Liu Y Y, et al. *Dyes Pigm.*, **2015**,**120**:136-146

[7] Li Q P, Jiang X, Du S W. *RSC Adv.*, **2015**,**5**:1785-1789

[8] Cheng L, Zhang L M, Gou S H, et al. *CrystEngComm*, **2012**, **14**:3888-3893

[9] Garcia-Zarracino R, Hpfl H. *J. Am. Chem. Soc.*, **2005**,**127**: 3120-3130

[10]Yang J X, Qin Y Y, Cheng J K, et al. *Cryst. Growth Des.*, **2014**,**14**:1047-1056

[11]Cheng L, Zhang L M, Cao Q N, et al. *CrystEngComm*, **2012**,

14:75027510

[12]Chen N, Li M X, Yang P, et al. *Cryst. Growth Des.*, **2013**, **13**:2650-2660

[13]Kathalikkattil A C, Bisht K K, Núria A A, et al. *Cryst. Growth Des.*, **2011**,**11**:1631-1641

[14]Zhang K, Jin C, Sun Y C, et al. *Inorg. Chem.*, **2014**,**53**:7803-7805

[15]Khullar S, Mandal S K. *Cryst. Growth Des.*, **2014**,**14**:6433-6444

[16]Wang J, Luo J H, Zhao J, et al. *Cryst. Growth Des.*, **2014**, **14**:2375-2380

[17]Ying S M, Huang X H, Luo W K, et al. *Acta Crystallogr. Sect. C*, **2014**,**70**:375-378

[18]Cao L H, Wei Y L, Yang Y, et al. *Cryst. Growth Des.*, **2014**, **14**:1827-1838

[19]Gould J A, Bacsa J, Park H, et al. *Cryst. Growth Des.*, **2010**, **10**:2977-2982

[20]Kumar N, Khullar S, Singh Y, et al. *CrystEngComm*, **2014**, **16**:6730-6744

[21]Miyake R, Nakagawa Y, Hase M. *Cryst. Growth Des.*, **2014**, **14**:4882-4885

[22]Abdel-Rahman L H, Nasser L A E. *Transition Met. Chem.*, **2007**,**32**:367-373

[23]Li M L, Song H H. *J. Solid State Chem.*, **2013**,**206**:182-191

[24]Sheldrick G M. *Acta Crystallogr. Sect. A*, **2008**,**64**:112-122

[25]Flack H D. *Acta Crystallogr. Sect. A*, **1983**,**39**:876-881

[26]He W W, Yang J, Yang Y, et al. *Dalton Trans.*, **2012**,**41**:9737-9747

[27]Marinho M V, Yoshida M I, Guedes K J, et al. *Inorg. Chem.*, **2004**,**43**:1539-1544

[28]Pinta N D L, Madariaga G, Lezama L, et al. *Eur. J. Inorg. Chem.*, **2010**,**22**:3491-3497

[29]LIANG Li-Li(梁丽丽), XU Lei(徐磊), CHEN Fei-Jian(陈飞剑), et al. *Chinese J. Inorg. Chem.*(无机化学学报), **2015**,**31**(10):1993-2000

[30]Yan V V W, Lo K K W. *Chem. Soc. Rev.*, **1999**,**28**:323-334

[31]Cheng L, Wang J, Yu H Y, et al. *J. Solid State Chem.*, **2015**, **221**:85-94